Quality Management of Energy Storage VSG Based on Odd-Order Repetitive Control

Yifei SUN, Jinghua ZHOU, Shasha CHEN, and Tianfeng LAN

***Abstract*—As renewable energy integration reduces grid strength, energy storage virtual synchronous generator (VSG) control becomes critical for grid support. However, power quality challenges arise from nonlinear loads and background harmonics in distribution networks. This study addresses energy storage VSG's power quality limitations by proposing a sensor-free selective control strategy to optimize point of common coupling (PCC) voltage or grid current without altering existing VSG structures. An odd-order repetitive control technique reshapes harmonic impedance, supported by a grid-VSG harmonic impedance model. Two supplementary loops selectively suppress voltage/current harmonics, enhancing power quality management without external sensors or harmonic extraction modules. The method eliminates hardware additions while resolving VSG harmonic issues in micro-grids and large grids. Results demonstrate significant improvements in harmonic mitigation, enabling energy storage VSG systems to partially replace active power filters (APFs). This approach offers a cost-effective solution for harmonizing renewable integration with grid stability, broadening VSG applicability. Key innovations include dual-loop adaptive harmonic suppression and impedance reshaping through modified repetitive control, advancing sensor-less power quality enhancement in modern power systems. The strategy effectively balances grid support functionality with harmonic management, facilitating scalable renewable energy adoption.**

***Index Terms*—Harmonic impedance reshaping, odd-order repetitive control, power conversion system, power quality, virtual synchronous generator.**

Nomenclature

VSG	Virtual synchronous generator.
PCC	Point of common coupling.
APF	Active power filter.
ORC	Odd-order repetitive control.
RC	Repetitive control.
PCS	Power conversion system.
VI	Virtual impedance.
THD	Total harmonic distortion.
V2G	Vehicle-to-grid.
PMR	Proportional multi-resonant.
VPI	Vector proportional-integral.
PLL	Phase-locked loop.
PI	Proportional-integral.
PWM	Pulse width modulation.
$v_{ga,b,c}(v_g)$	Grid voltage.
$v_{oa,b,c}(v_o)$	PCS voltage.
$i_{ga,b,c}(i_g)$	Grid current.
$i_{oa,b,c}(i_o)$	VSG current.
L_g	Grid impedance.
IGBT	Insulate-gate bipolar transistor.
R_L	Linear load.
LC	Nonlinear load filter.
L_fC_f	PCS filter.
$i_{La,b,c}(i_L)$	Inductor currents of PCS.
v_{dc}	DC voltage.
i_{dc}	DC current.
$v_{a,b,c}$	Voltage of C_f.
θ_{PLL}	Grid angle.
P_e	Average active power.
Q_e	Average reactive· power.
ω_c	Power filter cutoff frequency.
P_m	Mechanical power of VSG.
P_{ref}	Reference active power.
J	Rotational inertia.
D	Damping of the governor.
K_f	Active power droop coefficient.
ω_n	Rated angular frequency.
ω	Angular frequency of VSG.
θ	Output angular of VSG.
Q_m	Total reactive power reference.
Q_{ref}	Reactive power reference.
K_V	Reactive power droop coefficient.
K_Q	Excitation regulation coefficient.
V_{ref}	Reference voltage (peak).
V	Grid voltage (peak).
E_p	VSG internal electromotive force (peak).

Manuscript received January 13, 2025; revised February 23, 2025 and March 20, 2025; accepted April 19, 2025. Date of publication September 30, 2025; date of current version May 12, 2025. This work was supported in part by Beijing Municipal Natural Science Foundation under Grant L242007. (*Corresponding author: Jinghua Zhou.*)

Y. Sun and S. Chen are with School of Electrical and Control Engineering, North China University of Technology, Beijing 100043, China (e-mail: sunyifei@mail.ncut.edu.cn; chenshasha77@126.com).

J. Zhou is with Beijing Laboratory of New Energy Storage Technology, Beijing Municipal Education Commission and North China University of Technology, Beijing 100043, China (e-mail: zjh@ncut.edu.cn).

T. Lan is with Shanghai Electrical Apparatus Research Institute(Group) Co., Ltd., Shanghai 200333, China (e-mail: lantf@seari.com.cn).

Digital Object Identifier 10.24295/CPSSTPEA.2025.00019

e_{VSG}	VSG internal electromotive force.
m_{abc}	Modulation wave signals.
$G_{\mathrm{u}}(s)$	Voltage PI regulator.
$Z_{\mathrm{v}}(s)$	VI-component.
k_{c}	Current proportional coefficient.
$G_{\mathrm{i}}(s)$	Closed-loop transfer functions.
$Z_{\mathrm{o}}(s)$	Output impedance of VSG.
$Z_{\mathrm{g}}(s)$	Grid impedance.
Z_{o}^{h}	VSG h-th harmonic impedance.
Z_{g}^{h}	Grid h-th harmonic impedance.
$M_{\mathrm{rc}}(s)$	RC internal model.
$M_{\mathrm{orc}}(s)$	ORC internal model.
$G_{\mathrm{orc}}(z)$	ORC discrete implementation.
T_{s}	Discretization time.
$P_{\text{non-load}}$	Nonlinear load power.
L_{v}, R_{v}	VI parameters.

I. Introduction

WITH the rapid development of modern power systems, the integration of power electronic converters into microgrids and the main grid has introduced challenges such as reduced damping, weak inertia, and insufficient transient voltage support, which affect grid stability. The power conversion system (PCS), serving as the interface between energy storage devices and the grid/load, is a key component in energy storage systems. Among various control strategies, the energy storage virtual synchronous generator (VSG) is a promising solution to address these challenges[1], [2]. Moreover, the integration of nonlinear loads into distribution networks has worsened harmonic pollution, leading to significant power quality issues. These include increased line losses, transformer overheating, and mechanical vibrations, which threaten the stable operation of the grid. Therefore, further research on power quality management for energy storage VSGs is urgently needed.

Fig. 1 illustrates the harmonic suppression strategies for different types of inverters, which will be discussed separately. Research on power quality harmonic suppression methods for converters has predominantly focused on grid-following converters. Since these converters are current-controlled sources, suppressing internal harmonics (self-generated harmonic currents) is relatively straightforward. Techniques from [3]–[5] can effectively mitigate the harmonic currents they produce. [6] proposed a direct adaptive control strategy, achieving effective harmonic suppression of grid-connected converter output currents. External harmonic currents can be compensated for by installing passive filters or centralized active power filters (APFs) [7]. However, these solutions may introduce resonance problems and require additional inductive/capacitive components, which increase both system costs and maintenance complexity. To independently suppress external harmonic currents caused by nonlinear loads, a harmonic current compensation based on frequency-domain repetitive control was proposed in [8], aiming to counteract the harmonic currents generated by nonlinear loads. Additionally, by applying appropriate PCC

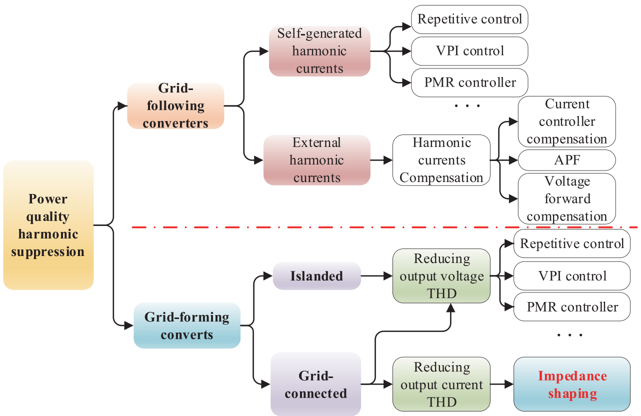

Fig. 1. Different harmonic suppression methods.

voltage feedforward control, the harmonic impedance of the inverter can be driven to infinity [9], significantly improving the power quality at the PCC point and providing some of the effects of an APF.

However, grid-forming energy storage converters exhibit voltage control characteristics, which differ from the current control characteristics of grid-following converters. As a result, traditional harmonic suppression methods designed for grid-following converters cannot be directly applied to energy storage VSG. Current research on power quality management for energy storage VSGs can be categorized into two main scenarios: islanded and grid-connected.

In islanded mode, VSGs act as voltage sources and should maintain the highest possible output voltage quality. The control objectives for energy storage VSG in islanded operation are clear. [10] proposed using third-order general integrator strategies to separate harmonic currents, which are then combined with variable virtual impedance to provide voltage harmonic compensation fed forward into the modulation wave, thereby reducing output voltage THD. However, this strategy alters the VSG's virtual impedance (VI), which is generally undesirable in practical applications, as VI also serves critical functions such as current limiting and grid strength adaptation, should not be easily changed. [11] proposed a control strategy involving adaptive VI to address this issue during fault conditions, thereby enhancing the VSG's output voltage quality. [12] introduced a method based on impedance angle estimation, enabling optimized VI adjustments to improve the output voltage quality when multiple VSGs operate in parallel under islanded conditions. [13] proposed a VSG quasi-harmonic voltage feedforward control method based on the rated and sampled voltages, which significantly reduces the harmonic impedance of the VSG, bringing it closer to an ideal voltage source. This improvement enhances the output voltage quality; however, it does not provide the capability to optimize the output current quality. [14] utilized repetitive control and a voltage-current harmonic extraction module to obtain harmonic information. This information is then multiplied by a variable coefficient to reshape the VSG's harmonic impedance, addressing the voltage harmonic suppression issue in islanded microgrids. However, this strategy does not account for hardware real-time constraints. Repetitive control itself is already resource-intensive for digital processing controllers, and with the addition of the complex harmonic extraction module, there is a risk that the algorithm may not complete within the required time under high switching frequency conditions. [15] eliminated the voltage-current harmonic extraction and adopted PMR in the inner loop of the VSG. By setting different controller coefficients, voltage and current harmonics are compensated separately. This strategy involves more parameters, compared to [14], it significantly improves software running speed and enhances practical applicability. The strategy has been successfully applied in V2G interconnected systems. [16] proposed an optimization control strategy for off-grid energy storage converters based on the internal model principle of repetitive control. This strategy is simple to design and does not require harmonic current extraction; however, it has not been thoroughly tested on grid-forming energy storage converters and is limited to voltage harmonic suppression. Additionally, [17] compared the performance of model predictive control in suppressing VSG output harmonics under resistive load conditions, demonstrating lower harmonic distortion compared to conventional control.

In grid-connected, the situation becomes more complex, the power quality optimization objective can be divided into two aspects:

- Optimizing the converter's output current;
- Optimizing the converter's output voltage.

The issue then becomes whether the harmonic current flows to the grid or to the grid-forming energy storage converter. If the optimization goal is to optimize the converter's output current, the majority of the harmonic current flows to the grid. However, if the goal is to optimize the converter's output voltage, the majority of the harmonic current flows into the converter, which then acts as an APF to supply harmonic current to the nonlinear loads. Based on this concept, [18]–[21] have established a harmonic impedance model for grid-forming energy storage converters and proposed a harmonic current distortion suppression method based on impedance shaping, which optimizes the grid current. These studies propose adding reactors at the PCC point to reduce the harmonic impedance between the PCC and the converter, thereby adapting to a wide range of grid impedance variations and optimizing the grid current. However, this strategy is challenging to implement in practice and requires additional hardware costs, such as low-latency data communication for relevant data acquisition. If the goal is to optimize the PCC voltage, research on this subject is limited, the relevant strategies can refer to the control of grid-forming energy storage VSGs in islanded operation[10]–[16]. [22] proposed adding harmonic voltage and current feedback control loops into modulation wave based on the existing VSG control framework to suppress converter output voltage harmonics. This strategy requires external load current sampling to obtain current and voltage harmonics, and the design of harmonic feedback control loop parameters is complex, involving numerous control parameters.

Existing research primarily concentrates on harmonic extraction and impedance reshaping strategies, which incur additional hardware costs and require the integration of multiple harmonic extraction and calculation modules. This paper proposes a harmonic suppression controller for grid-forming energy storage converters, utilizing the internal model principle and harmonic impedance reshaping. The innovations of this paper are as follows:

1) It respects the existing hardware design of energy storage converters and achieves PCC voltage optimization or output current optimization without adding extra voltage or current sensors.

2) Most previous studies have separated PCC voltage optimization and output current optimization, requiring harmonic extraction modules[18]–[21]. The proposed control strategy in this paper does not require harmonic extraction modules. Users can flexibly choose to suppress current or voltage harmonics, and the controller parameter design is simple.

The structure of this paper is organized as follows: Section II formulates the system model under investigation and introduces the impedance equivalent model of the energy storage VSG. Section III proposes a novel control, developed based on the impedance equivalent model, utilizing odd-order repetitive control. Section IV presents experimental validation of the proposed control strategy, demonstrating its accuracy and practical feasibility. Finally, Section V concludes the paper, summarizing the key findings and implications of the study.

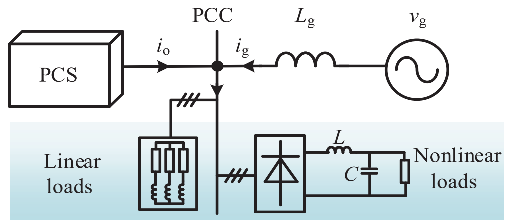

Fig. 2. System diagram of the energy storage converter.

II. System Structure and Equivalent Impedance Model

A. System Structure Under Study

The system configuration of the energy storage converter is depicted in Fig. 2. This simplified schematic outlines the connection between the PCS and the grid. The left represents the PCS device, with its output side connected to the grid through the PCC. Positioned to the right of the PCC, the inductor L_g symbolizes the grid impedance.

B. Energy Storage VSG Control

Fig. 3(a) illustrates the main circuit diagram of the PCS. The circuit topology employs a three-phase six-switch structure, where S1 to S6 represent IGBTs, and L_f and C_f denote the filter inductance and filter capacitance, respectively. The system samples the DC voltage v_{dc}, DC current i_{dc}, inductor currents i_{La}, i_{Lb}, and i_{Lc}, as well as the output currents i_a, i_b, and i_c. The voltages on both sides of the AC switch are v_a, v_b, v_c, v_{ga}, v_{gb},

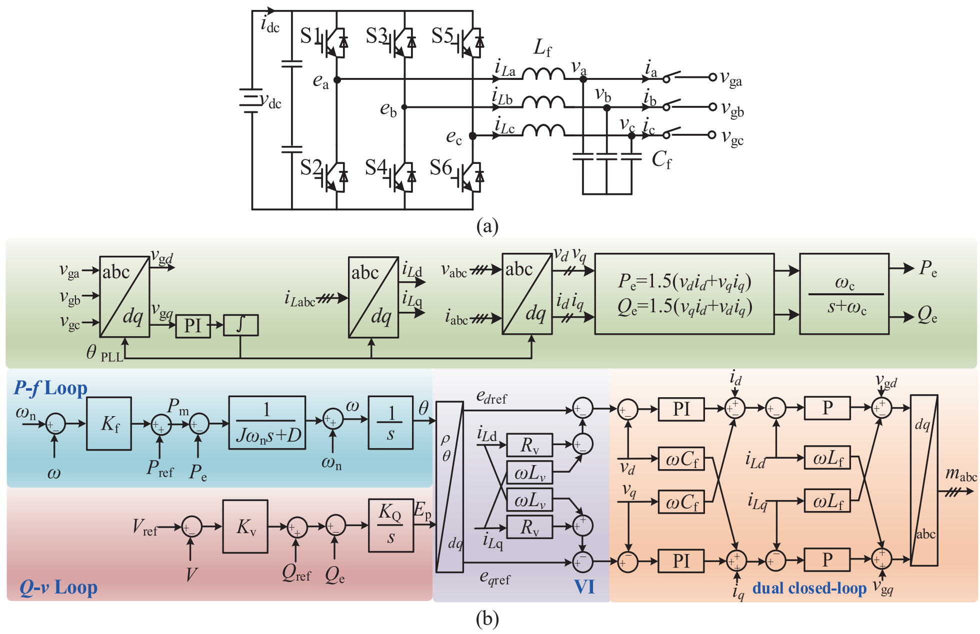

Fig. 3. Main circuit of PCS and VSG control block diagram. (a) Main circuit, (b) Control structure of VSG.

and v_{gc}.

Fig. 3(b) illustrates the control strategy of the VSG. The energy storage VSG control algorithm consists several modules, including the phase-locked loop (PLL), power calculation and filtering, *P-f* loop, *Q-v* loop, VI, and dual closed-loop control.

The instantaneous electromagnetic power output from the VSG is calculated using the three-phase instantaneous power theory as shown in Fig. 3(b). The average electromagnetic power P_e and reactive power Q_e of the VSG are derived by passing through a first-order low-pass filter with a cutoff frequency ω_c.

In the *P-f* loop, the primary frequency regulation function is achieved by simulating the behavior of a synchronous generator governor. J and D represent the rotational inertia and damping of the governor, respectively. The mathematical expressions for these are:

$$P_m = P_{ref} + K_f(\omega_n - \omega) \tag{1}$$

P_m represents the mechanical power of VSG, while P_{ref} is the reference active power. K_f denotes the active power-frequency droop coefficient. ω_n represent the rated angular frequency. In the *P-f* loop, the functions of inertia and damping are modeled by the rotor dynamics equation of a synchronous generator [1]. The mathematical expression for the first-order transfer function is:

$$P_m - P_e - D(\omega - \omega_n) = J\omega\frac{d\omega}{dt} \approx J\omega_n\frac{d\omega}{dt} \tag{2}$$

In the *P-f* loop, the expression for the VSG output angular velocity and angle is given by:

$$d\theta = dt = \omega \tag{3}$$

In the *Q-v* loop, the primary voltage regulation function is achieved by simulating the reactive power voltage droop characteristic of a synchronous generator. Q_m represents the total reactive power reference of the VSG, and its mathematical expression is:

$$Q_m = Q_{ref} + K_V(V_{ref} - V) \tag{4}$$

In the *Q-v* loop, the output voltage control is realized by simulating the excitation regulator of a synchronous generator. The mathematical expression is:

$$E_p = K_Q\int(Q_m - Q_e)dt \tag{5}$$

Within the *Q-v* loop, the reference voltage amplitude E_p is generated based on the output angle θ from the *P-f* loop. Through a coordinate transformation, the internal reference voltage for the VSG is derived. This reference voltage is then processed through VI and a dual closed-loop control to generate the modulation wave signals m_{abc}. These modulation signals are compared with carrier signals, which ultimately producing pulse signals that control the switches S1 to S6.

C. VSG Equivalent Impedance Model

The equivalent voltage-current control diagram of the VSG in the *abc* coordinate system is depicted in Fig. 4. The internal electromotive force of the VSG, denoted as e_{VSG}, is synthesized using e_o and angle θ, as shown in Fig. 3(b). The voltage proportional-integral (PI) regulator is represented by $G_u(s)$, whose expression is provided in (6). Additionally, k_c denotes the proportional gain of current inner-loop. The k_{pwm} represents the equivalent gain of the inverter bridge and can be considered a constant value of 1. $Z_v(s)$ is the VI component, and its expression is given in (7).

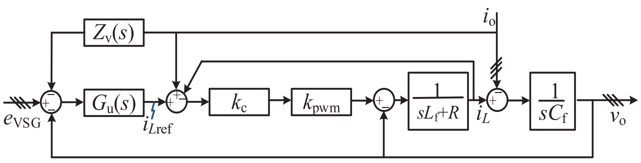

Fig. 4. Traditional VSG control equivalent voltage-current dual-loop control block diagram.

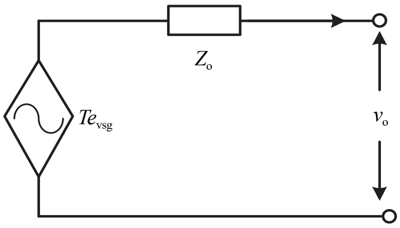

Fig. 5. VSG equivalent voltage source diagram.

$$G_u(s) = k_p + \frac{k_i}{s} \tag{6}$$

$$Z_v(s) = L_v(s) + R_v \tag{7}$$

The closed-loop transfer functions of the current loop and voltage loop can be derived from Fig. 4 as follows:

$$G_i(s) = \frac{i_L}{i_{Lref}} = \frac{k_c k_{pwm} \dfrac{1}{sL_f + R}}{1 + k_c k_{pwm} \dfrac{1}{sL_f + R}} \tag{8}$$

$$v_o(s) = \frac{G_u(s)G_i(s)}{Cs + G_u(s)G_i(s)}[e_{VSG}(s) - i_o(s)Z_v(s)] - \frac{1}{Cs + G_u(s)G_i(s)} i_o(s) \tag{9}$$

From (8) and (9), the voltage and current control loops of the traditional VSG can be equivalently modeled as a controllable voltage source with an external impedance, as shown in Fig. 5. Here, T and Z_o are defined by (10).

$$\begin{cases} T(s) = \dfrac{G_u(s)G_i(s)}{Cs + G_u(s)G_i(s)} \\ Z_o(s) = \dfrac{G_u(s)G_i(s)Z_v(s) + 1}{Cs + G_u(s)G_i(s)} \end{cases} \tag{10}$$

As illustrated in Fig. 5, the harmonic equivalent circuit of the VSG, load, and grid is further depicted in Fig. 6. The nonlinear load is modeled as a harmonic current source. In the absence of any special control, the harmonic impedance of the VSG, $Z_o^h(s)$, is equal to the grid impedance, $Z_o(s)$. The harmonic impedance of the grid is denoted as $Z_g^h(s) = Z_g(s)$.

Based on (10), the bode plot of the output impedance of the VSG and the grid is shown in Fig. 7. In Zone 1, where the VSG output impedance is greater than the grid output impedance, the grid absorbs a larger portion of the harmonic currents introduced by the nonlinear load. Conversely, in Zone 2, where the VSG output impedance is smaller than the grid output impedance, the VSG absorbs a larger portion of the harmonic currents from the nonlinear load.

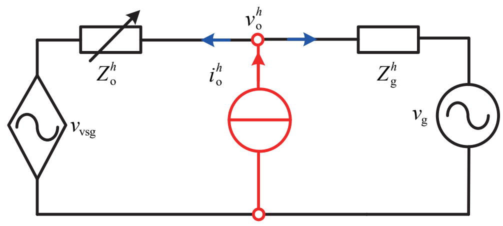

Fig. 6. Harmonic equivalent circuit diagram of VSG, load and grid connection.

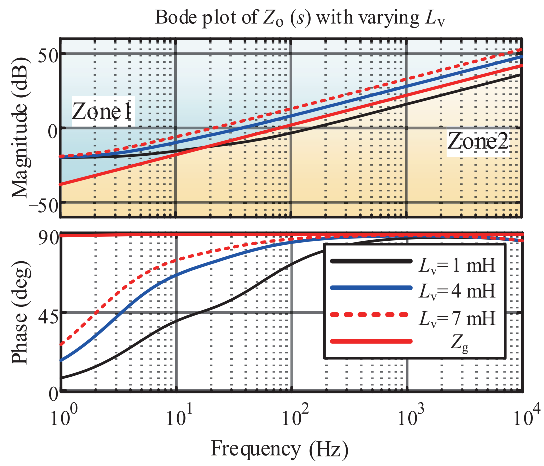

Fig. 7. Bode plot of VSG output impedance and grid impedance.

If the harmonic impedance of the VSG can be adjusted across different harmonic frequency bands, it would enable effective harmonic suppression and allow targeted control of harmonic current flow. This capability would facilitate the achievement of various control objectives by optimizing the distribution of harmonic current, offering an adaptable solution for different operational conditions.

III. Harmonic Impedance Reshaping Strategy Based on Odd-Order Repetitive Control

A. Principle of Odd-Order Repetitive Control

The basic principle of odd-order repetitive control is derived from the internal model principle, which introduces poles corresponding to targeted harmonic frequencies into the feedback loop. This internal model matches the dynamic characteristics of external periodic disturbance signals, enabling the control system to achieve near-zero steady-state error tracking for periodic reference signals and effectively suppress harmonic disturbances.

Fig. 8 presents a comparative illustration of the internal model structures used in traditional repetitive control (RC) and odd-order repetitive control (ORC). Here, u denotes the

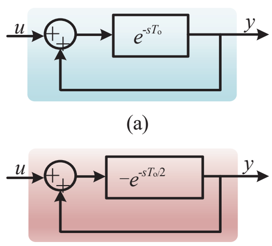

Fig. 8. Internal models of repetitive control. (a) RC internal model, (b) ORC internal model.

reference input signal, y is the output of the controller's internal model, T_o denotes the fundamental period of reference signal, and s denotes the differential operator.

The transfer functions of the internal models for the RC and ORC are given as follows:

$$M_{rc}(s)=\frac{e^{-sT_o}}{1-e^{-sT_o}}=\frac{1}{e^{sT_o}-1} \tag{11}$$

$$M_{orc}(s)=\frac{-e^{-sT_o/2}}{1+e^{-sT_o/2}}=\frac{-1}{e^{sT_o/2}+1} \tag{12}$$

As demonstrated in (11) and (12), the ORC utilizes $T_o/2$ storage units per cycle, representing a 50% reduction compared to the RC implementation. This structural advantage significantly lowers computational complexity while reducing hardware processor load. To extend the analysis of $M_{orc}(s)$, the following derivation is presented:

$$M_{orc}(s)=-\frac{1}{2}+\frac{4}{T}\sum_{k=1,3,5,7,\ldots}^{2n-1}\frac{s}{s^2+(k\omega_o)^2} \tag{13}$$

According to (13), M_{orc} is equivalent to multiple parallel PR controllers, and its internal model characteristics cover the fundamental frequency and its odd-order harmonic frequency bands of sine signals. This feature provides a theoretical basis for optimizing and shaping the impedance characteristics of the VSG [23].

Fig. 9 illustrates a comparison of the amplitude-frequency responses of the RC and ORC. The results demonstrate that at odd harmonic frequencies, the bandwidth of ORC (ω_{orc}) is twice that of RC (ω_{rc}) [24]. This implies that when the frequency fluctuates, the controller based on ORC internal model has stronger adaptability than the controller based on the RC internal model.

As shown in Fig. 2, the harmonic components are predominantly odd-order. The ORC not only requires fewer hardware resources, but also delivers superior performance in harmonic suppression. Based on this observation, this paper proposes a harmonic impedance reshaping strategy based on odd-order repetitive control, to exploit its advantages in power quality management.

Since the controller design is implemented in the discrete domain, the ORC controller is implemented as shown in Fig. 10. The transfer function expression is provided in (14).

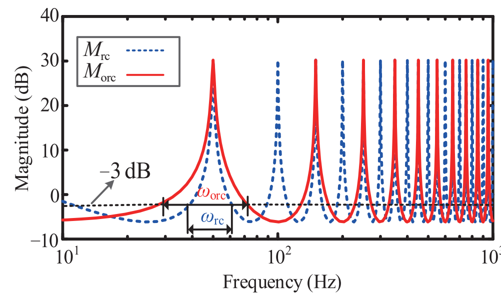

Fig. 9. Comparison of amplitude-frequency characteristics between RC and ORC.

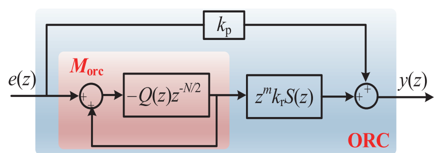

Fig. 10. Odd-order repetitive control discrete domain implementation.

$$G_{ORC}(z)=\frac{-Q(z)z^{-N/2}}{1+Q(z)z^{-N/2}}z^m k_r S(z)+k_p \tag{14}$$

The functions of each component in (14) are explained as follows:

- $e(z)$: Error signal;
- $y(z)$: Controller output;
- k_p: Proportional controller in parallel with the odd-order repetitive control;
- k_r: Internal gain coefficient of the odd-order repetitive control;
- $Q(z)$: Internal constant of the odd-order repetitive controller, or a zero-phase low-pass filter;
- $S(z)$: Low-pass filter;
- z^m: Phase lead compensation;
- N: Represents the sampling point period, where $N=f_s/f_g$, with f_s being the switching frequency and f_g being the grid frequency.

The proportional controller k_p effectively improves the dynamic response performance of the system, while the internal gain coefficient k_r adjusts the amplitude of the output signal, to ensure stability. The internal constant $Q(z)$ plays a crucial role in maintaining the stability of the system. The low-pass filter $S(z)$ further enhances the system's stability by attenuating high-frequency gains. Furthermore, the phase lead compensation z^m compensates for the phase delay introduced by $S(z)$ and the controlled system, ensuring that the system's phase characteristics in the frequency domain meet the design requirements.

B. The Proposed Controller Design

The power quality management control strategy based on ORC is illustrated in Fig. 11.

Compared with Fig. 3(b), the proposed control strategy achieves both voltage and current harmonic mitigation by adding only two simple loops and a three-way switch. When the

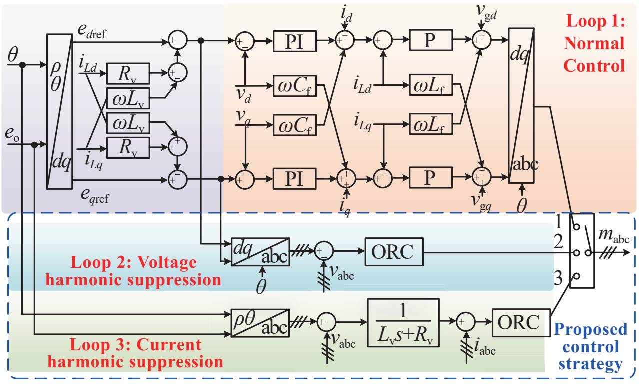

Fig. 11. The proposed control strategy.

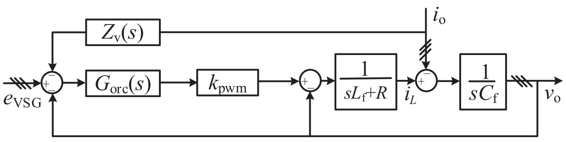

Fig. 12. VSG voltage harmonic suppression control block diagram.

switch is in position 1, the energy storage converter operates in the traditional grid-connected mode; when in position 2, the converter activates the voltage harmonic suppression; and in position 3, the converter performs current harmonic suppression. The proposed strategy significantly simplifies the software structure, enabling multifunctional harmonic mitigation while enhancing system flexibility and adaptability. For the ORC parameter design, readers can refer to [25], [26].

C. Analysis of the Proposed Controller's Capabilities

1) Voltage Harmonic Suppression Loop

The control block diagram of the voltage harmonic suppression loop, based on ORC control strategy is shown in Fig. 12. This loop is designed primarily as a voltage control loop, utilizing the ORC method. While the structure also allows for the addition of a current control loop in the subsequent stage, the focus of this paper is specifically on the design of the voltage loop. Thus, the current control loop is not discussed further in this study. This streamlined focus on the voltage loop ensures that the core functionality of the proposed strategy is fully explored, while the current loop remains a secondary consideration for future research.

The output impedance of the voltage harmonic suppression loop is given by:

$$Z_{out}(s)=\frac{v_o}{i_o}=\frac{\dfrac{1}{sC_f}+\dfrac{sL+R}{s^2LC_f+sRC_f}}{1+G_{orc}(s)k_{pwm}Z_v(s)} \tag{15}$$

Fig. 13 illustrates the magnitude-frequency characteristics of the output impedance Z_o of the grid-forming power conversion system and the grid output impedance Z_g in the frequency domain. The blue curve represents Z_o, which displays a notch filter characteristic at odd harmonic frequencies (e.g., 1st, 3rd, 5th, etc.). In contrast, the red straight line represents Z_g, which increases linearly with frequency.

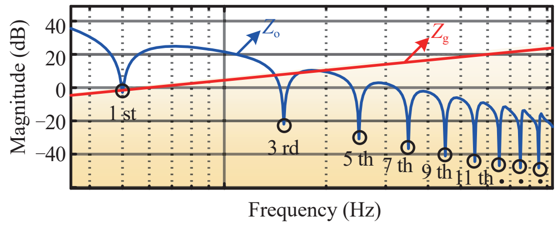

Fig. 13. The Magnitude-frequency characteristic curve of the VSG voltage harmonic suppression.

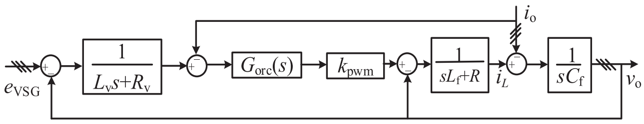

Fig. 14. VSG current harmonic suppression control block diagram.

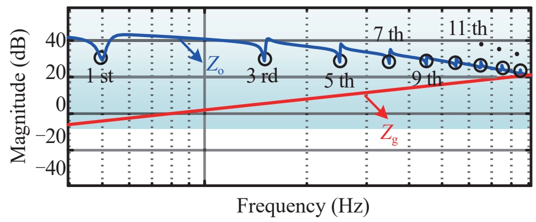

Fig. 15. The magnitude-frequency characteristics curve of the VSG current harmonic suppression.

At those odd harmonic frequencies, the significant reduction in Z_o and the relatively high Z_g cause harmonic currents to flow primarily into the PCS for absorption and suppression. This behavior indicates that the PCS can effectively absorb harmonic currents at these frequencies by optimizing its output impedance characteristics. Consequently, the proposed strategy improves power quality and reduce harmonic pollution at the PCC.

2) Current Harmonic Suppression Loop

The control block diagram of the current harmonic suppression loop, based on the ORC strategy, is shown in Fig. 14.

The output impedance of the current harmonic suppression loop is as follows:

$$Z_{out}(s)=\frac{v_o}{i_o}=\frac{sL_f+R+\dfrac{1}{sC_f}}{1+G_{orc}(s)k_{pwm}\dfrac{1}{L_vs+R_v}} \tag{16}$$

Fig. 15 shows the magnitude-frequency characteristics of the output impedance Z_o and the grid output impedance Z_g when using loop 3. At odd harmonic frequencies, Z_o is significantly higher than Z_g, causing the harmonic current to primarily flow into the grid rather than the PCS. This behavior indicates that by optimizing its output impedance characteristics, the PCS can effectively reject harmonic currents at odd harmonic frequen-

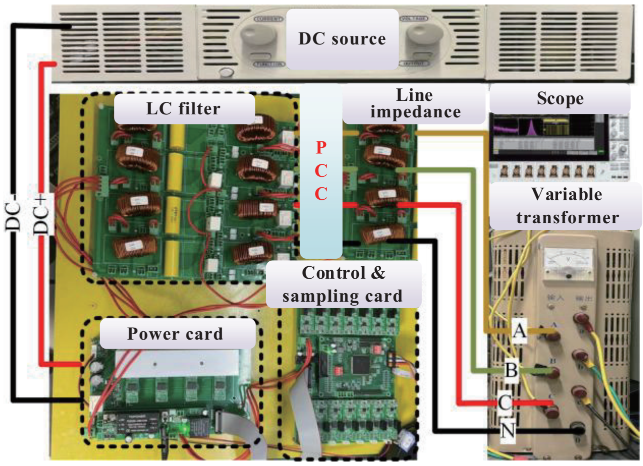

Fig. 16. Hardware platform.

TABLE I
POWER CIRCUIT PARAMETERS

Parameter	Value
DC voltage v_{dc}	75 V
AC voltage RMS v_g	38 V
Rated power P_n	300 VA
Line impedance L_g	3 mH
Linear load R_L	4.8 Ω
Nonlinear load R_{non}	12 Ω
Nonlinear load filter L	0.01 H
Nonlinear load filter C	0.001 F
Energy storage inverter L_f	1 mH
Energy storage inverter C_f	10 e−6 F
Filter damping resistor R_d	1 Ω
IGBT switching frequency	10 kHz

cies, thereby improving the output current quality of the PCS.

IV. Experimental Verification

To evaluate the efficacy of the proposed control strategy, a DC/AC experimental platform was developed, as depicted in Fig. 16. The platform consists of essential components such as the power module, control and sampling cards, LC filter, line impedance module, voltage regulator, and oscilloscope. The power circuit parameters are listed in Table I, and the control parameters are provided in Tables II and III.

A. Harmonic Suppression Capability of the Proposed Control Strategy

Fig. 17 presents the waveforms of the PCC point voltage, grid current, and VSG output current under various control strategies. The tested strategies include:

(a) Operation with a nonlinear load connected without any optimization;

TABLE II
VSG CONTROL PARAMETERS

Parameter	Value
Discretization time T_s	1/10 k
Rated angular frequency ω_n	314 rad
Active power frequency droop coefficient K_f	47.7 W/rad·s^{-1}
Inertia J	0.01*T_s kg·m^2
Damping coefficient D	0.5 Nm·s·rad^{-1}
Reactive power voltage droop coefficient K_v	300 Var/V
Excitation regulator coefficient K_Q	0.1*T_s
Virtual impedance R_v	0.1 Ω
Virtual impedance L_v	1 mH
Current loop proportional coefficient P	3
Voltage loop proportional coefficient PI	0.02 0.1*T_s

TABLE III
PROPOSED CONTROLLER PARAMETERS

Parameter	Value
Voltage harmonic suppression controller	
k_p	0.02
$Q(z)$	0.98
N	200
m	8
k_r	0.01
Current harmonic suppression controller	
k_p	0.05
$Q(z)$	0.98
N	200
m	200
k_r	0.08
$S(z)$	$\frac{0.002z^4+0.009z^3+0.013z^2+0.009z+0.0022}{z^4-2.69z^3+2.87z^2-1.4z+0.26}$

(b) Application of loop 2 for PCC voltage optimization using ORC as the inner model;

(c) Application of loop 3 for VSG current optimization using ORC as the inner model;

(d) Application of loop 2 for PCC voltage optimization using RC as the inner model;

(e) Application of loop 3 for VSG current optimization using RC as the inner model.

Fig. 18 illustrates the THD analysis of the PCC voltage, grid current, and VSG output current under various conditions. The results are as follows:

(a) THD when a nonlinear load is connected without any optimization;

(b) THD after implementing loop 2 for PCC voltage optimization using ORC as the inner model;

(c) THD after implementing loop 3 for VSG current optimization using ORC as the inner model;

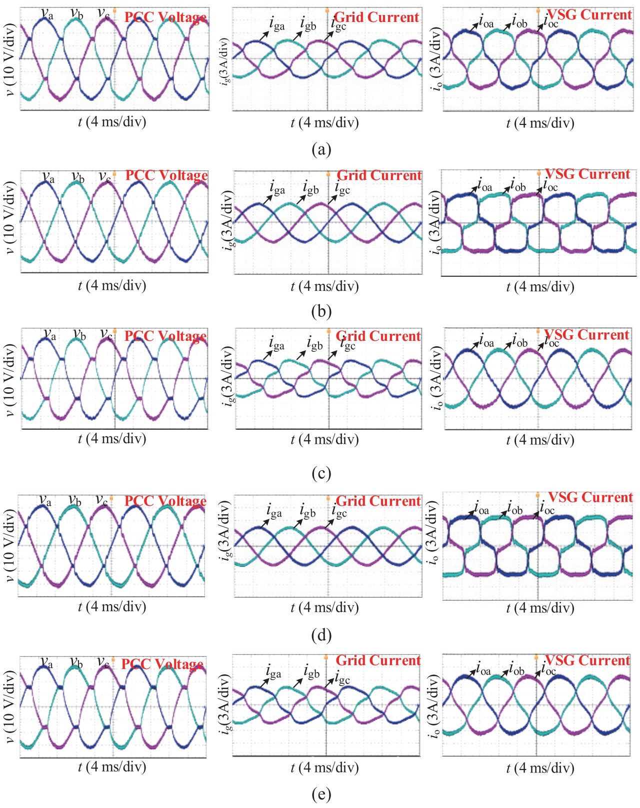

Fig. 17. Waveforms of PCC voltage, grid current, and VSG output current. (a) Loop 1, (b) Loop 2-ORC, (c) Loop 3-ORC, (d) Loop 2-RC, (e) Loop 3-RC.

(d) THD after implementing loop 2 for PCC voltage optimization using RC as the inner model;

(e) THD after implementing loop 3 for VSG current optimization using RC as the inner model.

Under linear load conditions, where no nonlinear loads are present, the PCC voltage, grid current, and VSG output current can maintain sinusoidal waveforms. However, when the system is connected to a nonlinear load without any optimization, the THD of the PCC voltage increases to 6.32% (Fig. 18(a)), and both the grid current and VSG output current exhibit significant distortion, with THD values of 6.38% and 13.29%, respectively. Furthermore, the distribution of harmonic currents is largely influenced by the output impedance of the VSG and the grid impedance. Without a control strategy, the harmonic current distribution remains unchanged, making it challenging to improve power quality.

When loop 2 (PCC voltage optimization using ORC as the inner model) is applied, the quality of the PCC voltage and grid current improves. The PCC voltage THD reduces from 6.32% (Fig. 18(a)) to 3.02% (Fig. 18(b)), and the grid current THD decreases from 6.38% (Fig. 18(a)) to 4.63% (Fig. 18(b)). However, this optimization strategy results in a higher THD for the VSG output current, which increases from 13.29% (Fig. 18(a)) to 18.71% (Fig. 18(b)), as more harmonic current is allocated to the VSG.

Switching to loop 3 (VSG current optimization) significantly improves the VSG output current quality, with the THD decreasing from 13.29% (Fig. 18(a)) to 5.97% (Fig. 18(b)). However, this leads to an increase in the grid current THD,

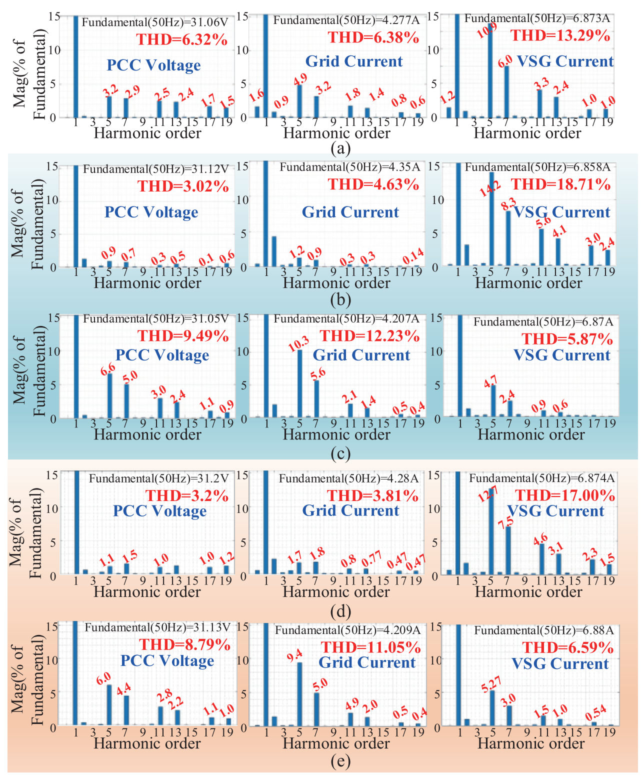

Fig. 18. THD analysis of PCC voltage, grid current, VSG output current. (a) Loop 1, (b) Loop 2-ORC, (c) Loop 3-ORC, (d) Loop 2-RC, (e) Loop 3-RC.

from 6.38% (Fig. 18(a)) to 12.23% (Fig. 18(b)), and the PCC voltage quality deteriorates, with the THD rising from 6.32% to 9.49%.

Additionally, the performance of the ORC and RC inner models is compared (Fig. 18(d) and (e)). Although the RC model offers similar performance in terms of THD reduction, it does not provide significant improvements over ORC, especially in terms of optimization. The THD values for the PCC voltage and VSG output current using RC (3.2% and 6.59%, respectively) are only marginally different from those achieved with ORC (3.02% and 5.89%). Moreover, the use of RC significantly impacts processor speed, making it a less desirable choice for this application.

In conclusion, the proposed control strategy demonstrates a trade-off between different optimization objectives: Loop 2 focuses on optimizing the PCC voltage and grid current, while loop 3 prioritizes optimizing the VSG output current. The optimal choice depends on the system's operational requirements and the specific power quality goals.

B. Subharmonics and Interharmonics Analysis

For power systems operating at a fundamental frequency of 50 Hz, the instantaneous voltage and current waveforms analyzed by discrete fourier transform typically consist of various frequency components. Components at integer multiples of the fundamental frequency are defined as harmonics, while those at non-integer multiples of the fundamental frequency are termed interharmonics. Additionally, frequency components below the fundamental frequency are known as subharmonics,

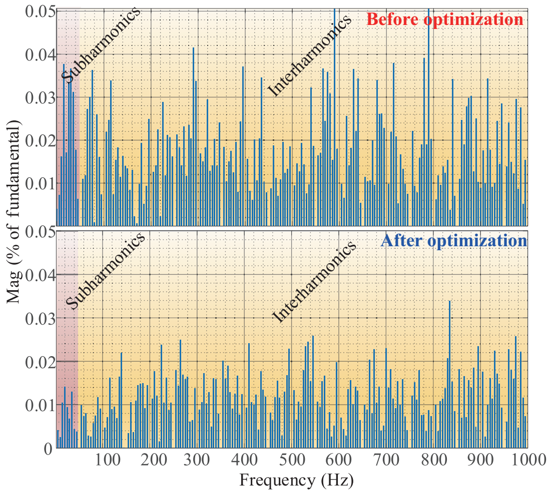

Fig. 19. Analysis of interharmonics and subharmonics in the PCC voltage.

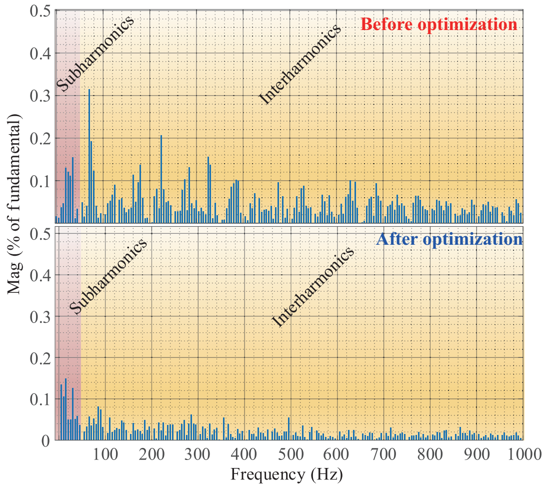

Fig. 20. Analysis of interharmonics and subharmonics in the VSG current.

which can also be considered as interharmonics existing between DC and the fundamental frequency. In this study, experimental data were recorded using an oscilloscope with a sampling depth of 1 m. To meet the required frequency resolution for interharmonic measurement (5 Hz), continuous sampling over 10 fundamental periods (0.2 s for a 50 Hz fundamental) was performed. The sampled data were subsequently imported into MATLAB/Simulink for fast Fourier transform analysis.

Fig. 19 shows the analysis of interharmonics and subharmonics in the PCC voltage before and after PCC voltage optimization. Before optimization, the maximum magnitude of subharmonics reaches approximately 0.35% of the fundamental component, while interharmonics reach around 0.4%. After optimization, the magnitudes of subharmonics and interharmonics decrease, both dropping below approximately 0.2%. This demonstrates that the proposed optimization strategy effectively mitigates both interharmonic and subharmonic distortion, significantly enhancing PCC voltage quality. Fig. 20 illustrates the interharmonics and subharmonics in the VSG

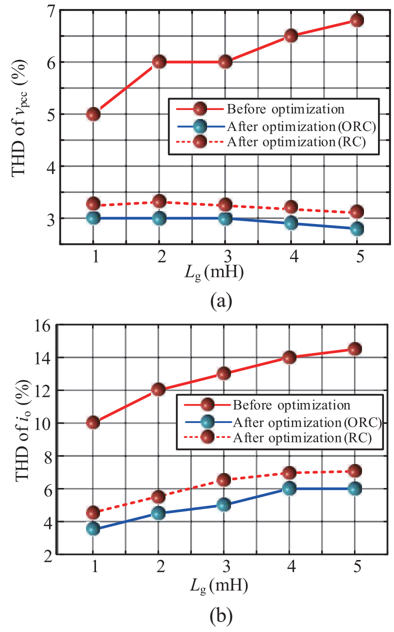

Fig. 21. Comparison of optimization effects under grid impedance variations. (a) Loop 1 vs loop 2, (b) Loop 1 vs loop 3.

output current before and after optimization. Initially, the subharmonic and interharmonic components in the current reach as high as approximately 0.5% and 0.4% of the fundamental component, respectively. After the proposed optimization, these magnitudes are significantly reduced, with the highest values of subharmonics and interharmonics falling below about 0.1%. This indicates that the proposed control method also effectively improves the VSG output current waveform, substantially reducing harmonic distortion.

The proposed method employs ORC, which provides a relatively wide bandwidth as illustrated in Fig. 9. As a result, this approach exhibits low sensitivity to subharmonics and interharmonics caused by frequency fluctuations and achieves effective suppression.

C. Robustness of the Proposed Control Strategy

To assess the robustness of the proposed control strategy, we evaluated its optimization effects on the PCC voltage and VSG output current under varying grid impedance and nonlinear load power conditions.

1) Grid Impedance Variation

Fig. 21(a) illustrates the optimization results for the PCC voltage as the grid impedance changes from 1 mH to 5 mH. Before optimization, the PCC voltage THD fluctuates significantly with changes in grid impedance. However, after optimization (using ORC), the PCC voltage THD is consistently maintained below 3%.

Fig. 21(b) presents the optimization results for the VSG output current under the same grid impedance variations. Prior to optimization, the minimum value of output current THD is 10%, but after optimization (ORC), the maximum output current THD remains below 6%.

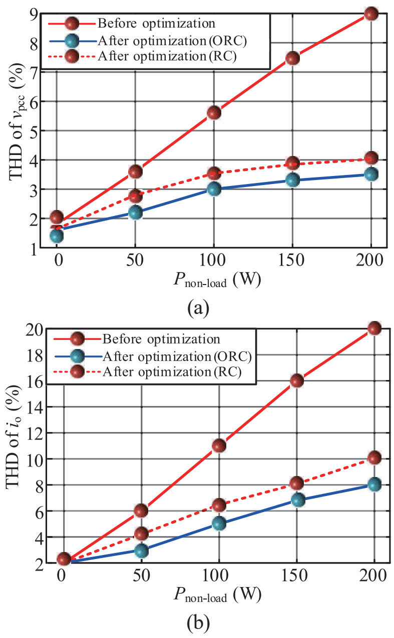

Fig. 22. Comparison of optimization effects of the proposed control strategy under variations in nonlinear load power. (a) Loop 1 vs loop 2, (b) Loop 1 vs loop 3.

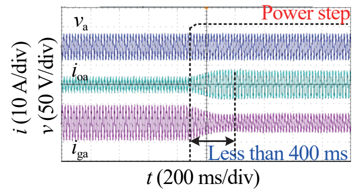

Fig. 23. Dynamic response of traditional control under power step change.

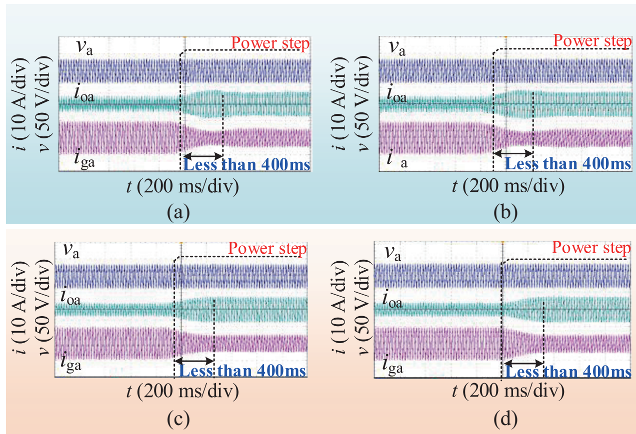

Fig. 24. Dynamic response of the proposed control strategy under power step change. (a) Loop 2-ORC, (b) Loop 3-ORC, (c) Loop 2-RC, (e) Loop 3-RC.

2) Nonlinear Load Power Variation

Fig. 22(a) shows the optimization results for the PCC voltage as the nonlinear load power varies from 0 to 200 W. Before optimization, the PCC voltage THD increases approximately linearly with the nonlinear load power, reaching a maximum of 9%. After applying ORC optimization, the PCC voltage THD is consistently kept below 3.5%.

Similarly, Fig. 22(b) shows the optimization results for the VSG output current under the same load power variations. Before optimization, the output current THD increases nearly linearly with the load power, peaking at 20%. After optimization, the output current THD does not exceed 8%.

The results obtained with RC optimization are similar to those from ORC; however, the optimization performance with RC is slightly inferior. These results clearly demonstrate that the proposed power quality management strategy exhibits robust performance. Despite parameter variations in the system, it effectively suppresses harmonics and maintains output power quality.

D. Dynamic Performance of the Proposed Control Strategy

To evaluate the dynamic performance of the proposed control strategy, the active power reference of the VSG is stepped from 100 W to 300 W. The following figures present the PCC voltage, VSG output current, and grid current under different control strategies: Fig. 23 shows the results for loop 1 (without optimization); Fig. 23(a) presents the results for loop 2 using ORC as the inner model (PCC voltage optimization); Fig. 22(b) shows the results for loop 3 using ORC as the inner model (VSG output current optimization); Fig. 24(c) demonstrates the results for loop 2 using RC as the inner model (PCC voltage optimization); Fig. 24(d) illustrates the results for loop 3 using RC as the inner model (VSG output current optimization).

As observed in Figs. 22 and 23, the dynamic response time of the energy storage VSG remains consistently below 400 ms, regardless of the control method employed. This is consistent with the analysis presented in [27], which emphasizes that the dynamic response of VSG control is primarily influenced by the outer loop control. The proposed strategy modifies the inner loop, and thus does not affect the system's dynamic performance.

V. Conclusion

This paper proposes an odd-order repetitive controller based on the internal model principle, which reshapes the harmonic impedance of the VSG while preserving its fundamental functions. This approach enhances the power quality management capability of the energy storage VSG. The proposed method allows for selective control of either voltage optimization or output current optimization, enabling the energy storage VSG to operate similarly to an APF without the need for additional external sensors, thus achieving "one machine with multiple uses". Consequently, this technology can not only complement traditional APFs in power quality management but also offers great flexibility.

References

[1] Z. Qing-Chang and G. Weiss, "Synchronverters: Inverters that mimic synchronous generators, " in *IEEE Transactions on Industrial Electronics*, vol. 58, no. 4, pp. 1259–1267, Apr. 2011.

[2] O. Babayomi, Z. Li, and Z. Zhang, "Distributed secondary frequency and voltage control of parallel-connected VSCs in microgrids: A predictive VSG-based solution," in *CPSS Transactions on Power Electronics and Applications*, vol. 5, no. 4, pp. 342–351, Dec. 2020.

[3] G. Zhang, Q. Zhao, Y. Ye, A. Wang, S. Wen, and Y. Wang, "Feedforward repetitive control for grid-tied inverters in microgrids: Analysis, design, and verification," in *IEEE Transactions on Industrial Electronics*, vol. 71, no. 9, pp. 11239–11249, Sept. 2024.

[4] Q.-N. Trinh and H.-H. Lee, "An advanced current control strategy for three-phase shunt active power filters," in *IEEE Transactions on Industrial Electronics*, vol. 60, no. 12, pp. 5400–5410, Dec. 2013.

[5] Z. Wu, X. Guo, and B. Wang, "Coordinated control strategy for cascaded current-source converter under unbalanced grid voltage," in *IEEE Transactions on Power Electronics*, vol. 39, no. 5, pp. 5439–5448, May 2024.

[6] G. V. Hollweg, P. J. D. de O. Evald, E. Mattos. L. C. Borin, R. V. Tambara, and H. A. Gründling, and W. Su, "A direct adaptive controller with harmonic compensation for grid-connected converters," in *IEEE Transactions on Industrial Electronics*, vol. 71, no. 3, pp. 2978–2989, Mar. 2024.

[7] X. Jiang, H. Yi, F. Zhuo, and Y. Li, "A stabilization strategy based on grid current feedforward for the harmonic oscillation of APF system," in *IEEE Journal of Emerging and Selected Topics in Power Electronics*, vol. 12, no. 2, pp. 2116–2129, Apr. 2024.

[8] Q.-N. Trinh and H.-H. Lee, "An enhanced grid current compensator for grid-connected distributed generation under nonlinear loads and grid voltage distortions," in *IEEE Transactions on Industrial Electronics*, vol. 61, no. 12, pp. 6528–6537, Dec. 2014.

[9] Q. Yan, X. Wu, X. Yuan, and Y. Geng, "An improved grid-voltage feedforward strategy for high-power three-phase grid-connected inverters based on the simplified repetitive predictor," in *IEEE Transactions on Power Electronics*, vol. 31, no. 5, pp. 3880–3897, May 2016.

[10] J. M. Alcala, M. Castilla, L. G. de Vicuña, J. Miret, and J. C. Vasquez, "Virtual impedance loop for droop-controlled single-phase parallel inverters using a second-order general-integrator scheme," in *IEEE Transactions on Power Electronics*, vol. 25, no. 12, pp. 2993–3002, Dec. 2010.

[11] A. H. Jafariazad, S. A. Taher, Z. D. Arani, M. H. Karimi, and J. M. Guerrero, "Adaptive supplementary control of VSG based on virtual impedance for current limiting in grid-connected and islanded microgrids," in *IEEE Transactions on Smart Grid*, vol. 15, no. 1, pp. 89–98, Jan. 2024.

[12] M. Aquib, A. S. Vijay, S. Doolla, and M. C. Chandorkar, "Model reference adaptive system based apparent power sharing in inverter based microgrids," in *IEEE Transactions on Energy Conversion*, vol. 37, no. 3, pp. 1987–1997, Sept. 2022.

[13] G. Li, W. Song, and X. Liu, "A quasi-harmonic voltage feedforward control for improving power quality in VSG-based islanded microgrid," in *IEEE Journal of Emerging and Selected Topics in Power Electronics*, vol. 12, no. 3, pp. 2994–3004, Jun. 2024.

[14] Q. Chen, "A Control Strategy of Islanded Microgrid With Nonlinear Load for Harmonic Suppression," in *IEEE Access*, vol. 9, pp. 39171–39181, 2021.

[15] D. Elik and M. E. Meral, "A coordinated virtual impedance control scheme for three phase four leg inverters of electric vehicle to grid (V2G)," in *Energy*, vol. 246, p. 123354, May 2022.

[16] J. Zhou, Y. Sun, S. Chen, and T. Lan, "A fast repetitive control strategy for a power conversion system," in *Electronics*, vol. 13, no. 7, p. 1186, 2024.

[17] C. Zheng, T. Dragičević, and F. Blaabjerg, "Model predictive control-based virtual inertia emulator for an islanded alternating current microgrid," in *IEEE Transactions on Industrial Electronics*, vol. 68, no. 8, pp. 7167–7177, Aug. 2021.

[18] L. Zhou, Z. Shuai, Y. Chen, W. Wu, X. Zhou, K. Yan, and A. Luo, "Impedance-based harmonic current suppression method for VSG connected to distorted grid," in *IEEE Transactions on Industrial Electronics*, vol. 67, no. 7, pp. 5490–5502, Jul. 2020.

[19] W. Yang, M. Wang, S. Aziz, and A. Y. Kharal, "Magnitude-reshaping strategy for harmonic suppression of VSG-based inverter under weak grid," in *IEEE Access*, vol. 8, pp. 184399–184413, 2020.

[20] S. Li, J. Wu, G. D. Agundis-Tinajero, S. K. Chaudhary, J. C. Vasquez, and J. M. Guerrero, "A decomposed harmonic current suppression method for VSG-based microgrids connected to distorted grids," in *IEEE Transactions on Industrial Electronics*, vol. 71, no. 9, pp. 10669–10680, Sept. 2024.

[21] L. Zhou, S. Liu, Y. Chen, W. Yi, S. Wang, X. Zhou, W. Wu, J. Zhou, C. Xiao, and A. Liu, "Harmonic current and inrush fault current coordinated suppression method for VSG under non-ideal grid condition," in *IEEE Transactions on Power Electronics*, vol. 36, no. 1, pp. 1030–1042, Jan. 2021.

[22] G. Lou, Q. Yang, W. Gu, X. Quan, J. M. Guerrero, and S. Li, "Analysis and design of hybrid harmonic suppression scheme for VSG considering nonlinear loads and distorted grid," in *IEEE Transactions on Energy Conversion*, vol. 36, no. 4, pp. 3096–3107, Dec. 2021.

[23] Q. Zhao, H. Zhang, Y. Xia, Q. Chen, and Y. Ye, "Equivalence relation analysis and design of repetitive controllers and multiple quasi-resonant controllers for single-phase inverters," in *IEEE Journal of Emerging and Selected Topics in Power Electronics*, vol. 13, no. 3, pp. 3338–3349, Jun. 2025.

[24] S. Chen, Q. Zhao, S. Chen, and Y. Ye, "Modified PIMR-type ORC for odd harmonic current suppression in a single-phase grid-tied inverter," in *Proceedings of 2019 IEEE 8th Data Driven Control and Learning Systems Conference (DDCLS)*, Dali, China, 2019, pp. 1044–1048,

[25] J. Zhou, D. Fan, and Y. Sun, "Inertia-active power filter design based on repetitive control," in *Electronics*, vol. 13, no. 13, p. 2615, 2024.

[26] Y. Sun and J. Zhou, "Grid-tied inverter fractional-order phase compensation via odd repetition control," in *Proceedings of 2023 6th International Conference on Electrical Engineering and Green Energy (CEEGE)*, 2023, pp. 62–68.

[27] H. Wu, X. Ruan, D. Yang, X. Chen, W. Zhao, Z. Lv, and Q. Zhong, "Small-signal modeling and parameters design for virtual synchronous generators," in *IEEE Transactions on Industrial Electronics*, vol. 63, no. 7, pp. 4292–4303, Jul. 2016.

Yifei Sun was born in 1997 in China. He received his Bachelor's degree in electrical engineering from Zhongyuan University of Technology in 2019, and continued his studies at North China University of Technology, where he is currently a Ph.D. candidate in electrical engineering since 2022. His research focuses on power electronic converters and their applications.

From 2019 to 2022, he studied at Zhongyuan University of Technology, and since 2022, he has been working as a Ph.D. student at North China University of Technology. His current research interests include the design, control, and application of power electronic converters in various energy systems, with particular attention to grid-connected systems, renewable energy integration, and advanced control strategies.

His academic work has led to several published papers and conference presentations in the field of power electronics. He is dedicated to advancing the application of power electronics technologies for improving energy efficiency and power quality in modern electrical systems.

Zhou Jinghua is a professor and Ph.D. supervisor. He is a Senior Member of CPSS. His research interests include high-power power electronic conversion technology and grid-connected energy storage inverters.

Shasha Chen is a Ph.D. student whose research focuses on high-power power electronic conversion technology and power quality management.

Tianfeng Lan received the B.Eng. degree in electrical engineering and automation from Shanghai University, China, in 2013, and the M.Eng. degree in electrical engineering from the University of Sydney, Australia, in 2017. Since 2019, he has been serving as a Testing and Certification Manager at Shanghai Electrical Apparatus Research Institute (SEARI) Co., Ltd., where he leads technical evaluations and compliance assessments for power electronics systems. His research focuses on high-power energy storage converters, including topology optimization, grid-connected control strategies, and reliability enhancement for industrial-scale applications. He has contributed to multiple national-level certification standards for energy storage systems in China. Mr. Lan actively collaborates with industry partners to bridge advanced theoretical research with practical engineering solutions.